High Yield Dispersions of Large-Diameter Semiconducting Single-Walled Carbon Nanotubes with Tunable Narrow Chirality Distributions

Kevin S. Mistry,[†,‡] Brian A. Larsen,[†] and Jeffrey L. Blackburn[†,*]

[†]National Renewable Energy Laboratory, Golden, Colorado 80401, United States, and [‡]Department of Physics, University of Colorado, Boulder, Colorado 80309, United States

Supporting Information
Calculation of Dispersion Concentration and Yield for PFO-BPy

We calculated the concentration and yield of SWCNTs dispersed by PFO-BPy through a detailed gravimetric and spectroscopic approach. We define the dispersion concentration as the mass of nanotubes contained per milliliter of total solution (mg/ml) and the dispersion yield as the mass of dispersed *semiconducting* SWCNTs following centrifugation relative to the total mass of *semiconducting* SWCNTs found in the raw material before dispersion (% yield of s-SWCNTs). The yield can also be expressed as a total yield, which is defined as the mass of s-SWCNTs dispersed by PFO-BPy relative to the total mass of SWCNTs present in the raw material before dispersion.

Ideally, calculating the yield and concentrations of these dispersions could be made by simply comparing the absorbance of a sonicated dispersion before and after centrifugation. However, it is important to realize that the raw SWCNT soot that we use to make these dispersions contains much less than 100% SWCNTs by mass. There is a significant amount of amorphous carbon present in the raw soot, as well as the Ni and Co catalyst particles. Figure S1a compares the absorbance spectra for raw and highly purified SWCNTs at identical concentrations (0.12 mg/ml). To prepare the purified SWCNTs, 100 mg of SWCNTs are first refluxed for 16 hours in 4 M nitric acid, and then rigorously washed in a filtration apparatus (Teflon filter) with acetone, water, and 1 M sodium hydroxide to flush out non-nanotube carbon. Finally, the resulting nanotube paper is burned in air at 525 °C for ~30 seconds to thoroughly remove any remaining amorphous carbon. Thermogravimetric analysis (TGA) indicates that the resulting SWCNT paper is 97 ± 1% SWCNTs, with the remainder being Ni and Co catalyst particles.

In Figure S1a, each sample is sonicated in PFO-BPy/toluene for 30 minutes and *is not centrifuged following sonication*. It is immediately apparent that the absorbance spectrum for the raw soot dispersion contains a significant background that rises into the UV that is absent for the purified dispersion. This background has been demonstrated in numerous studies to arise from amorphous carbon impurities, and can be roughly approximated by a power law fit (red dashed line). When this background is subtracted from the raw soot dispersion (Figure S1b), the resulting spectrum is dominated by the strong excitonic SWCNT transitions, and overlays well on top of the purified spectrum when appropriately normalized. There are slight deviations between the corrected raw spectrum and the purified spectrum that arise from:

1. The power law fit not being a perfect representation of the absorbance for the amorphous carbon
2. A slight reduction in the contribution of small diameter SWCNTs to the purified dispersion, due to the increased reactivity (and loss) of smaller diameter SWCNTs in the purification process.

Regardless of these minor deviations, we can use the ratio of the optical densities (or the integrated peak areas) of the two samples to determine that the SWCNTs contribute to ~31% of the optical density observed for the purified SWCNT sample. Correcting for the weight % of SWCNTs in the purified dispersion (97%), and running this analysis on five separate raw SWCNT dispersions, we calculate an average value of 30 ± 3% by mass of SWCNTs in the raw soot.

To further validate the analysis described above, and as a second check on this analysis, we used TGA to determine the mass of SWCNTs relative to the total mass of raw soot, as shown in Figure S1c. Several groups, including ours, have demonstrated that when raw SWCNT soot is burned in air, both amorphous carbon impurities and SWCNTs decompose at the same time due to the exothermic oxidation of metal catalyst impurities that leads to thermal runaway. Thermal runaway can be avoided by performing the TGA in a flowing CO_2 atmosphere, in which the decomposition/oxidation of all phases becomes endothermic. Figure S1c demonstrates that in flowing CO_2, two distinct thermal decompositions appear that are well separated by nearly 500 °C. Our extensive previous work, combining TGA and transmission electron microscopy, demonstrated that the first thermal decomposition can be assigned to amorphous carbon and the second decomposition can be assigned to SWCNTs. In the raw SWCNTs, the amorphous phase constitutes ~49% of the total mass loss, while the SWCNT phase constitutes ~38%. The residual mass observed above 1200 °C results from the oxidized Ni and Co catalyst particles. Previous X-ray diffraction (XRD) measurements in our group demonstrated that this phase consists primarily of NiO and CoO, but can also oxidize farther to Ni_2O_3 and Co_2O_3 at higher temperatures, resulting in mass increases of the catalyst phase of 127 – 136%. The residual mass of 9.9% yields a Ni/Co catalyst content of 7.5 ± 0.3%, close to the value of 6% utilized for the LV target material. Multiple TGA decompositions were measured to arrive at an average value of 36 ± 2% by mass of SWCNTs in the raw soot, a value slightly larger than the 30 ± 3% value estimated by absorbance. This discrepancy is understandable, since there could be amorphous carbon trapped within/between SWCNT bundles that isn't burned away within the first decomposition. Regardless, including an artificially high value obtained by TGA should only cause us to *underestimate* the ultimate dispersion yield that we calculate. **With this in mind, we calculate an average value for the SWCNT content of the raw soot of 33 ± 4% by mass, based on the average values of the absorbance and TGA measurements.**

We next set out to calculate an absorbance coefficient for the second semiconducting excitonic transitions (S_{22}). For this measurement, we first dispersed six different aliquots of the highly purified (97%) SWCNT material into 10 ml of PFO-BPy solution, using the same sonication regime described for the samples in the main manuscript. The samples were weighed on a Mettler-Toledo microbalance, and masses ranged from 0.139 mg to 1.165 mg. The resulting dispersions *were not centrifuged following sonication*, so that the mass of SWCNTs in each dispersion was accurately known. Absorbance spectra of three of these samples are shown in Figure S2a. The optical density at 937 nm (OD_{937} the peak of the S_{22} transition envelope) was used to generate an absorbance coefficient, ε, *via* Beers law: $A = OD_{937} = \varepsilon \ell c$, where ε is the absorbance coefficient with units of (ml mg^{-1} cm^{-1}), ℓ is the path length in centimeters and c is the concentration in mg/ml. Figure S2b plots OD_{937}, normalized to path length, versus the concentration of purified SWCNTs. The slope of the plot yields an absorbance coefficient, ε = 39.86 ± 0.69 (ml mg^{-1} cm^{-1}). Taking into account that the sample is not 100% SWCNTs, normalizing this value to the SWCNT content of 97 ± 1% yields ε = 41.10 ± 0.83 (ml mg^{-1} cm^{-1}).

The value of ε = 41.10 ± 0.83 (ml mg^{-1} cm^{-1}) is a valid absorbance coefficient for SWCNT dispersions containing the statistical ratio of s- and m-SWCNTs. Thus, this value must be adjusted for samples such as the PFO-BPy LV dispersions demonstrated in the manuscript that contain only s-SWCNTs. To adjust the absorbance coefficient accordingly, the absorbance spectrum was deconvoluted into the separate contributions of s- and m-SWCNTs. The s-SWCNT contribution was simply modeled by the PFO-BPY LV absorbance spectrum shown in Figure 1a of the main manuscript. To model the m-SWCNT contribution, we utilized the spectrum of a highly pure (> 99%) m-SWCNT sample produced in our lab by density gradient ultracentrifugation (DGU). Figure S2c shows the result of this deconvolution, and demonstrates that for a sample containing *only s-SWCNTs*, OD_{937} is ~85% of the value found for a sample containing the statistical ratio of s- and m-SWCNTs. **This analysis adjusts the absorbance coefficient to 34.94 ± 0.70 (ml mg^{-1} cm^{-1}) at the peak of the S_{22} transitions, ε_{937}, for dispersions containing only s-SWCNTs.**

We now have all of the numbers we need to calculate the concentration and yield of our PFO-BPy LV dispersions. First, we use the value for the absorbance coefficient determined above to estimate the

concentration of the dark PFO-BPy dispersion displayed in Figure 1a and 1b, noting that the OD_{937} = 1.41 and ℓ = 0.5 cm. **This analysis yields a concentration of 0.081 ± 0.002 mg/ml for the PFO-BPy dispersion shown in Figure 1a.** Next, using our estimation that the raw soot is comprised of 33 ± 4% SWCNTs, we can calculate the yield of s-SWCNTs dispersed by PFO-BPy. We start with the fact that our initial SWCNT loading for the sample in Figure 1a is 1.1 mg/ml, meaning that 0.363 mg/ml of SWCNTs are initially present in solution before processing, and only 2/3 of these SWCNTs (0.242 mg/ml) are semiconducting. Using the final concentration of the sample after centrifugation of 0.081 mg/ml, calculated above, we arrive at a yield of 33 ± 4%. **This analysis suggests that PFO-BPy selectively disperses ~33% of the s-SWCNTs initially present in the raw SWCNT soot, or ~22% of all SWCNTs initially present in the raw soot.**

To translate these numbers to a throughput, we consider that the high ink concentrations and material yields demonstrated above only require 30 minutes of sonication and 5 minutes of centrifugation. We have performed batch dispersions as large as 100 ml without observing any loss of selectivity. The centrifuge rotor used here (Beckman SW-31) has capacity for six tubes, with each tube holding a maximum of 39 ml, for a maximum capacity of 234 ml. If we consider a conservative estimate of performing two separate 100 ml batch sonications simultaneously (*i.e.* with two sonicators) and leaving 2 ml of solution in the bottom of every centrifuge tube following centrifugation, we arrive at 188 ml of retrieved solution. Using the concentration of 0.08 mg/ml calculated above, *this translates to a lab-scale throughput of ~15 mg of > 99% pure s-SWCNTs (<d> ≈1.3 nm) in under one hour*.
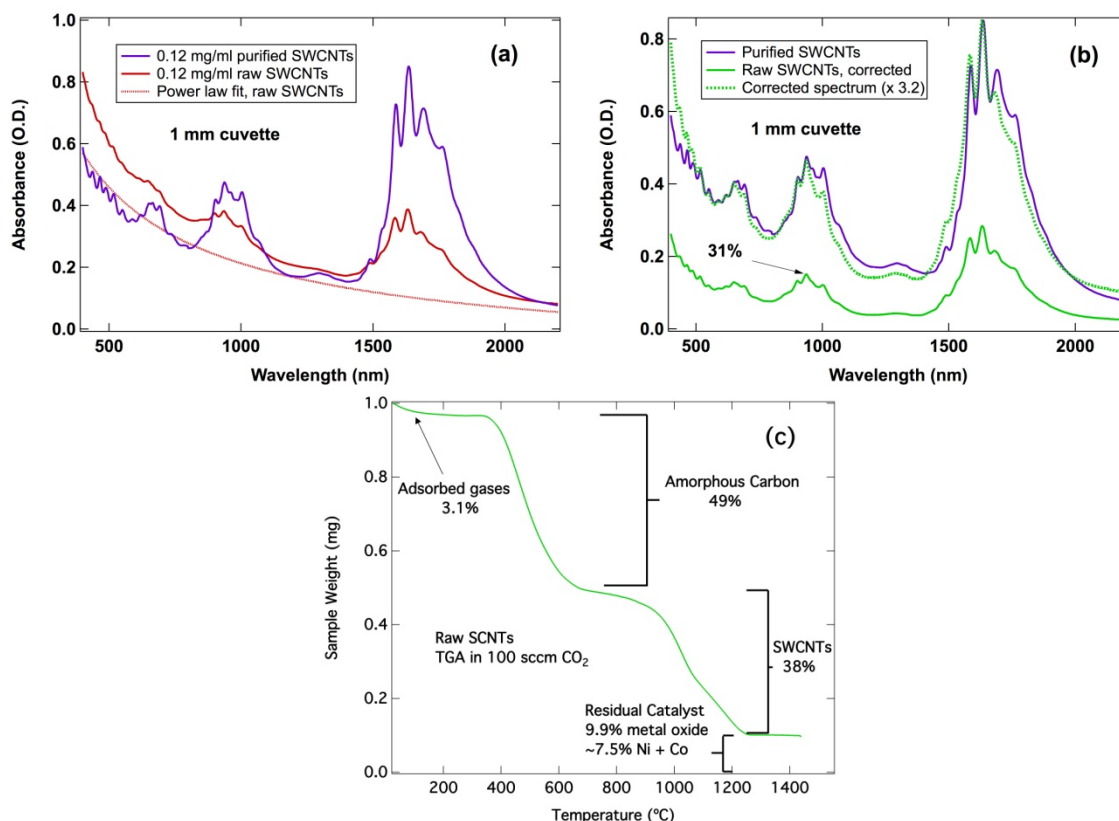

Figure S1. (a) Comparison of the absorbance spectra for raw and highly purified SWCNTs (97 ± 1 % SWCNTs) at identical concentrations. Each sample is sonicated in PFO-BPy/toluene for 30 minutes and is not centrifuged following sonication. The red dashed line illustrates a power law fit used to approximate the contribution of amorphous carbon impurities to the spectrum of the raw SWCNTs. (b) Comparison of the corrected absorbance spectrum for the raw soot (amorphous phase removed *via* subtraction of power law fit) to the spectrum of the

purified material. Both samples are total mass loadings of 0.12 mg/ml. The dashed green spectrum is the corrected raw spectrum multiplied by 3.2 to overlay with the purified spectrum, indicating a ~32% SWCNT content in the raw soot (when correcting for the fact that the purified material is 97% SWCNTs). (c) Thermogravimetric analysis (TGA) of raw LV SWCNTs in CO_2. The 5 mg sample was ramped at 10 °C per minute to 1440 °C and held for 10 minutes. The weight loss axis is normalized to a 1 mg sample for clarity. The weight losses associated with each separate component are labeled in the plot, demonstrating that the SWCNTs comprise ~38% of the total sample weight. Two TGAs of separate aliquots of the raw material returned an average value of 36 ± 2% SWCNTs by weight in the raw material. Combining the values obtained through spectroscopic and gravimetric analysis produces an average value of 33 ± 4% SWCNTs by weight in the raw soot.
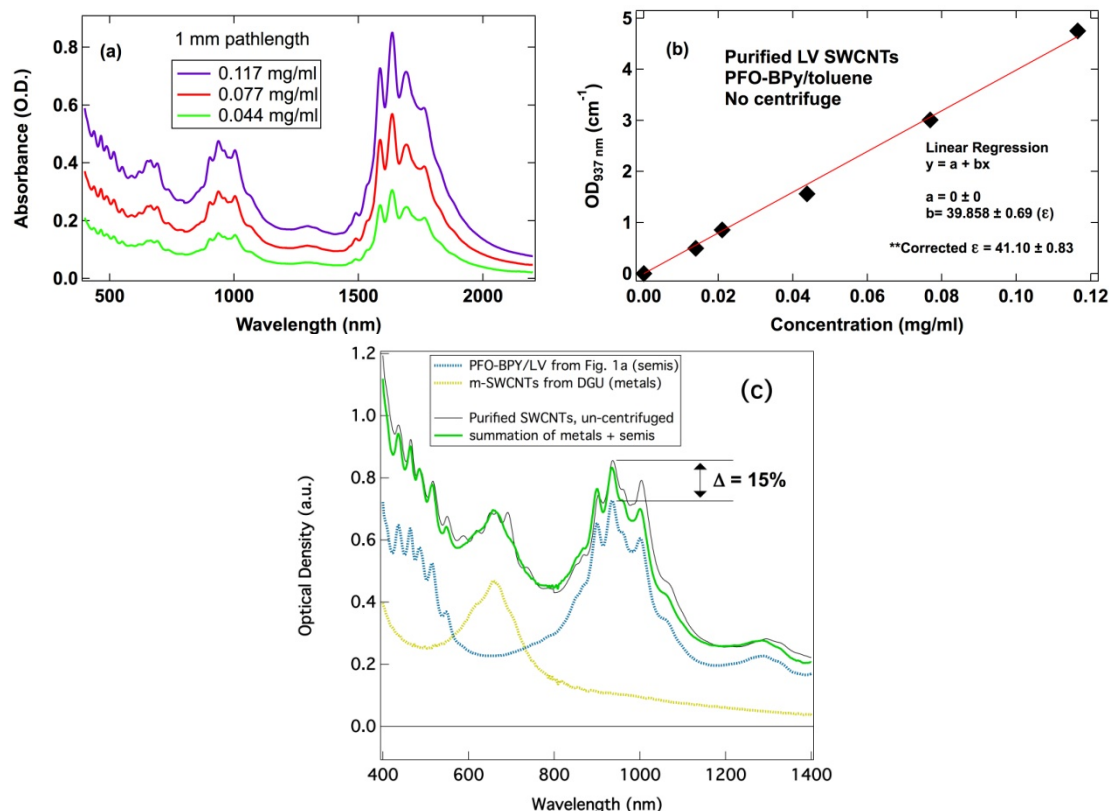

Figure S2. (a) Absorbance spectra of highly purified LV SWCNTs (~97% SWCNTs) dispersed in PFO-BPy/toluene and *not subjected to centrifugation*. (b) Absorbance (normalized to a 1 cm pathlength) at the peak of the S_{22} peaks (937 nm) for six different samples prepared in the same manner, as a function of sample concentration (mg/ml). The linear regression, shown in red, yields an absorbance coefficient at 937 nm of 39.86 ± 0.69 (ml mg^{-1} cm^{-1}). Correcting this number for the actual SWCNT mass (97 ± 1% of sample mass) yields a corrected value of 41.10 ± 0.83 (ml mg^{-1} cm^{-1}). (c) De-convolution of the absorbance spectrum of the purified SWCNT material into the contributions from s-SWCNTs and m-SWCNTs. The blue spectrum is a PFO-BPy LV dispersion containing only s-SWCNTs (semis) and the yellow spectrum is a > 99% m-SWCNT sample obtained *via* DGU (metals). The green spectrum is the sum of these spectra, which overlays well on top of the spectrum obtained from the purified SWCNTs dispersed in PFO-BPy and not centrifuged (black trace). This analysis allows us to correct the absorbance coefficient by multiplying by 85% to reach a final corrected value of 34.94 ± 0.70 (ml mg^{-1} cm^{-1}).
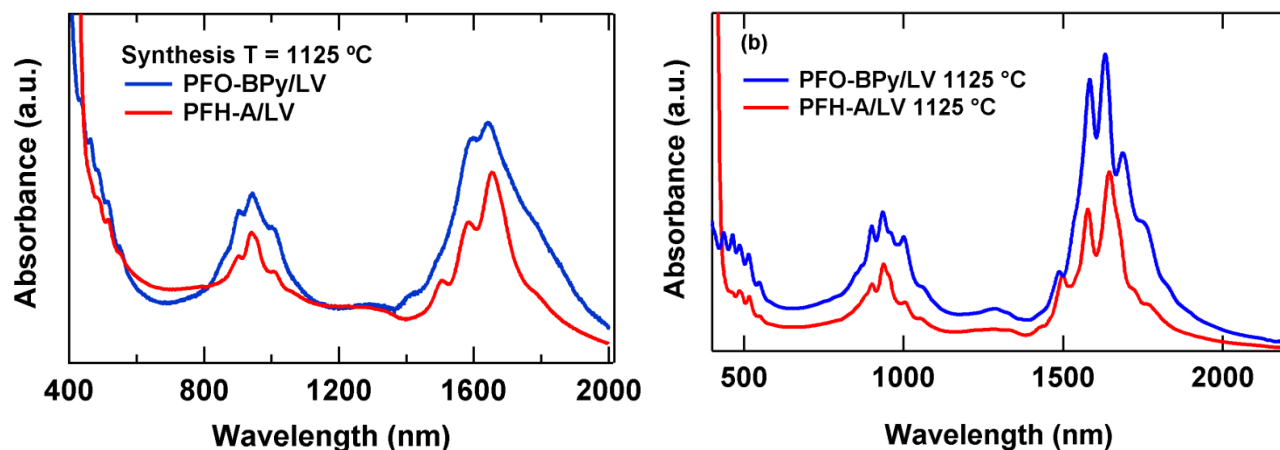
Figure S3. (a) Absorbance spectra of transparent thin films prepared by ultrasonic spraying of LV SWCNTs dispersed in toluene with either PFO-BPy or PFH-A. The PFH-A film suffers from more haze than the PFO-BPy, most likely due to scattering from excess PFH-A, producing a sloping background for the PFH-A absorbance spectrum. However, the comparison clearly demonstrates the narrower chirality distribution for PFH-A, in agreement with the PLE maps shown in the main manuscript. (b) Absorbance spectra of PFO-BPy and PFH-A dispersions of LV SWCNTs taken in a 1 mm path length cuvette to allow toluene background subtraction. Excitonic transitions in solution are clearly narrower than in films because SWCNTs are well isolated.

Vibronic Sidebands of s-SWCNTs in Absorbance Spectra (*e.g.* Figure 1a)

The peaks labeled with asterisks in Figure 1a are vibronic absorbance features related to optical transitions of dark (optically forbidden) excitons (center of mass momentum at the K point, thus momentum-forbidden) that are coupled to in-plane transverse optical (iTO) phonons, also known as the D band. We discussed this vibronic feature in detail for the (6,5) SWCNT in a recent Nano Letters publication.[1] These features are easy to distinguish in nearly-monochiral samples (Figure S4), but show up as broad peak envelopes in samples with multiple chiralities and may overlap with optically allowed transitions. The peaks in question arise from the second K-momentum dark exciton vibronic transitions. The energy of this feature always appears ~180 – 200 meV above the energy of the optically allowed transitions in question, since the dark exciton lies ~25 – 40 meV above the bright exciton. The peaks arising from the first (lowest energy) K-momentum dark exciton vibronic transitions are easily visible in the region of ~1200 to 1350 nm in the absorbance spectrum in Figure 1a, and those arising from the second dark exciton vibronic transitions are visible in the range of ~700 – 800 nm. The correlation of two shoulders in Figure 1a at 750 nm and 800 nm with semiconducting SWCNTs can be most easily seen by turning the 2D PLE map of Figure 2a into a 3D map and turning it on its side (Figure S5a). This produces a structured excitation profile of the semiconducting SWCNTs that demonstrates distinct peaks at ~750 nm and ~790 nm. Excitation slices also reveal these features very clearly (Figure S5b). For example, the excitation slice at 1555 nm emission wavelength reveals a prominent feature at 750 nm, due to the vibronic excitation of the second dark (K-momentum) exciton of the (11,7) SWCNT.
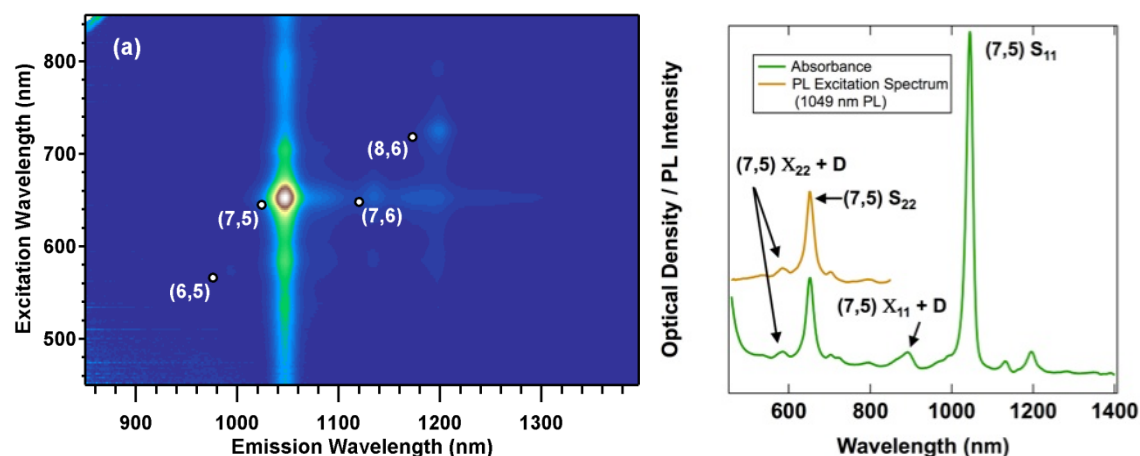

Figure S4. (a) PLE map of PFO-dispersed CoMoCAT SWCNTs (SG65 material). The sample is highly enriched in the (7,5) SWCNT, with small contributions from the (7,6), (8,6), and (6,5) SWCNTs. (b) Absorbance spectrum (green) and PL excitation spectrum (orange) of the same sample. Labels mark the first and second bright excitonic transitions (S_{11} and S_{22}) of the (7,5) SWCNT, as well as the first and second phonon-assisted dark excitonic transitions (X_{11} + D and X_{22} + D, where D is the iTO "D-band" phonon).
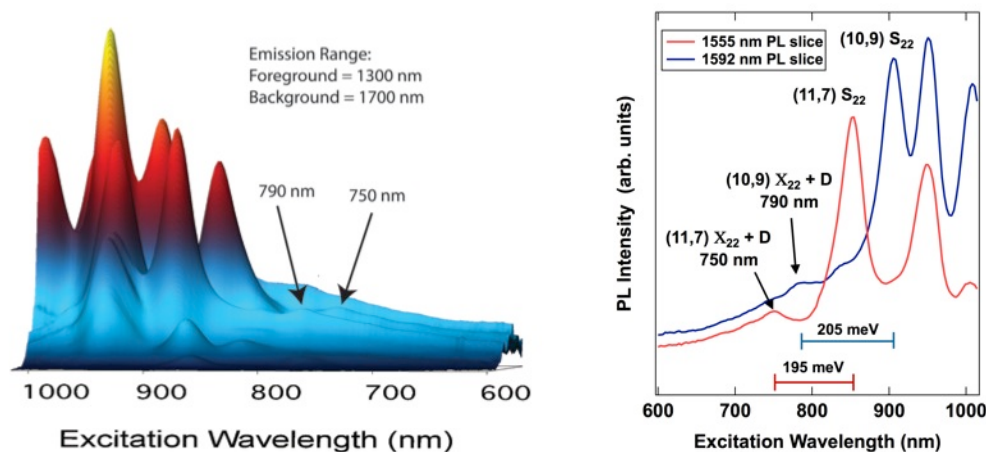
Figure S5. (a) Three-dimensional PLE map of PFO-BPy dispersed LV SWCNTs (synthesis T = 1125 °C) turned on its side to display the excitation spectra of all SWCNTs. The arrows point out two vibronic peaks due to phonon-assisted absorbance of the optically forbidden K-momentum exciton (X_2) *via* coupling to the D band phonon. (b) Excitation slices at 1555 nm and 1592 nm to highlight the vibronic sidebands of the (11,7) and (10,9) SWCNTs, at 750 nm and 790 nm, respectively.
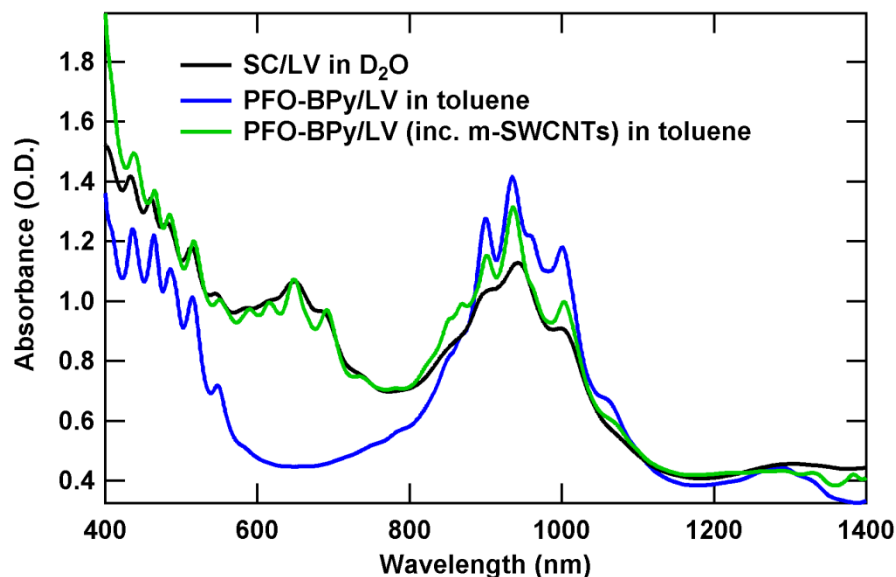

Figure S6. Absorbance spectrum of PFO-BPy/LV prepared to intentionally include m-SWCNTs (green). The absorbance spectra for SC/LV and PFO-BPy from Figure 1 are included for comparison.
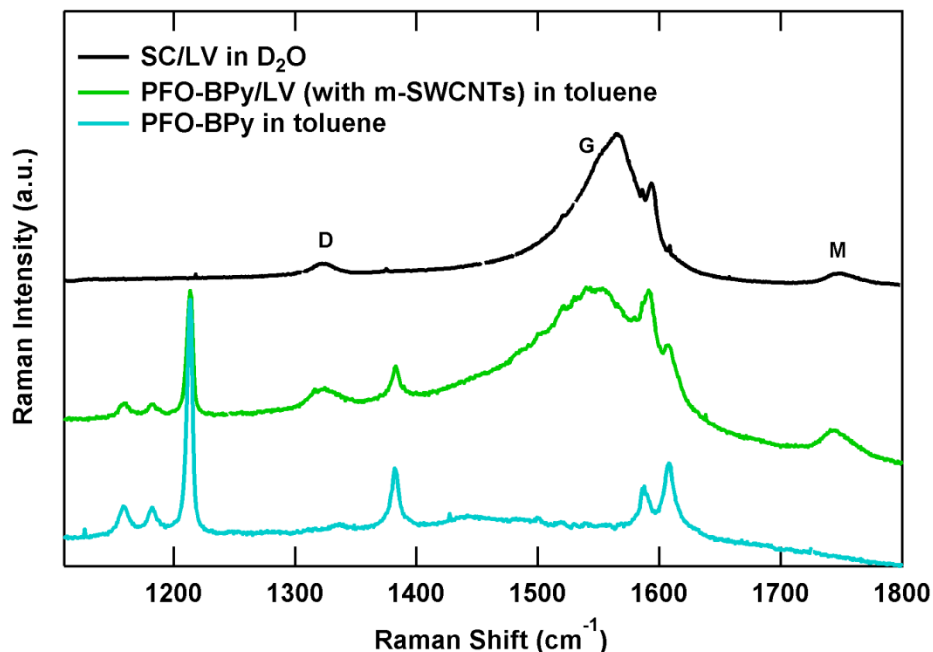
Figure S7a. Raman spectra showing metallic signatures in a solution of PFO-BPy/LV in toluene. Spectra have been offset for visibility. The concentration of PFO-BPy was higher than typical solutions and the LV SWCNTs were treated to remove metal catalyst and amorphous carbon impurities before being dispersed into solution in order to get m-SWCNTs to disperse as well. The D, G, and M bands become visible in this solution as well as the signatures from PFO-BPy/toluene.
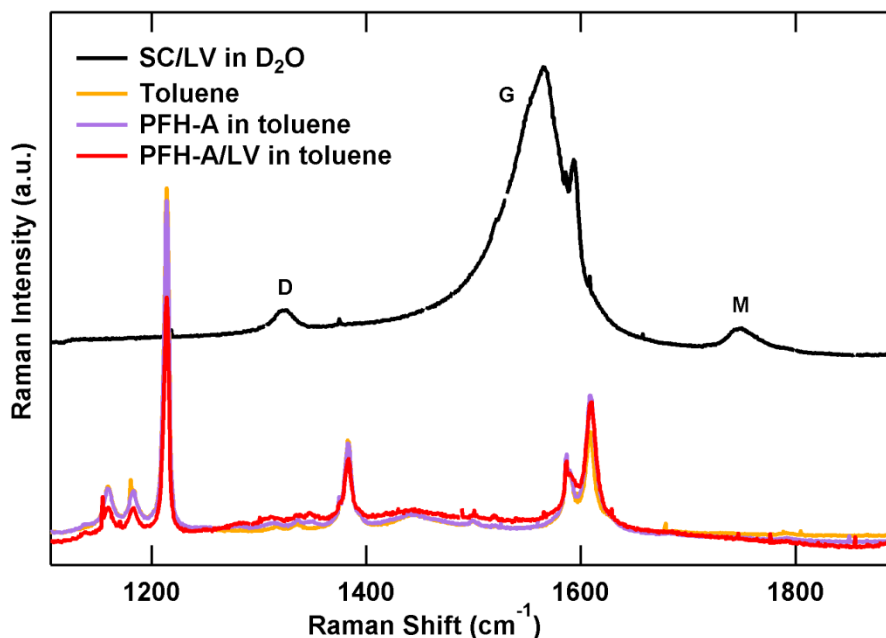

Figure S7b. Raman spectra of SC/LV in D_2O, PFH-A/LV in toluene, PFH-A in toluene, and neat toluene. Signatures of m-SWCNTs are clearly visible in the SC/LV sample and absent in the other three. Spectra have been offset for visibility. It appears that all of the non-SWCNT signatures are a result of the toluene.

Qualitative Evaluation of s-SWCNT Enrichment by Comparison to a Commercially Available Product

It is an important, but difficult, task to quantitatively evaluate the enrichment level of semiconducting or metallic SWCNTs produced by a given separation or dispersion procedure. Such information guides the expectations for a given material in device applications and also influences the interpretation of fundamental measurements that can be influenced by impurities with undesired electronic structure. We typically estimate the enrichment level of our LV SWCNTs by absorbance spectroscopy. Specifically, a comparison of the integrated areas underneath the S_{22} and M_{11} peak envelopes can afford an estimate of the semiconducting or metallic SWCNT percentages. Using this analysis on our LV SWCNTs dispersed with PFO-BPy and PFH-A, we estimate s-SWCNT enrichment levels of at least 99%. A more quantitative analysis becomes difficult, especially for s-SWCNTs, at high levels of enrichment, *e.g.* > 99%, due to spectral overlap of the M_{11} peaks with the S_{22} and S_{33} peak envelopes. Thus, absorbance cannot be used to assess whether or not a s-SWCNT enriched sample has the ppm-level m-SWCNT impurities required for applications such as digital logic.

In an attempt to qualitatively benchmark our polyfluorene dispersed LV s-SWCNTs, we compare our absorbance spectrum to that of (to our knowledge) the only commercially available large-diameter SWCNT product enriched in semiconducting nanotubes. This comparison is shown below in Figure S8. The spectrum of a sample that is sold as 99% s-SWCNTs, produced by Nanointegris *via* DGU of arc-discharge SWCNTs, was obtained directly from the Nanointegris Technical Data Sheet for their IsoNanotubes-S product: (http://www.nanointegris.com/en/downloads). The IsoNanotubes-S spectrum is shown in purple, while our PFO-BPy/LV sample is shown in green. We adjusted the absorbance and wavelength ranges of our spectrum to match those used by Nanointegris (the wavelength tick marks are included in our plot and overlay directly over the tick marks in the other plot). The absorbance axis is adjusted so that the peak intensity of the S_{22} envelope is equivalent for each spectrum, and the axis range is adjusted so that each axis covers the same fractional change in absorbance (*i.e.* a factor of 12 absorbance change over the displayed range). This normalization ensures that valid comparisons, free of artificial baseline manipulation, can be made between the spectra. The primary qualitative observation that can be made from this comparison is that the spectrum for our PFO-BPy dispersed LV SWCNTs has less structure, and a deeper valley, between the S_{22} and S_{33} peak envelopes where the M_{11} peaks are observed in mixed samples. This observation suggests that our PFO-BPy dispersed LV SWCNTs have an s-SWCNT enrichment level *at least* equivalent to, and likely higher than, this commercially available IsoNanotubes-S product that is quoted at a 99% s-SWCNT purity level. From this comparison, and our own analysis of the integrated S_{22}/M_{11} areas, we conclude that our polyfluorene-dispersed LV SWCNTs have s-SWCNT enrichment levels greater than 99.0%. Work to rigorously quantify the purity beyond this level is ongoing.
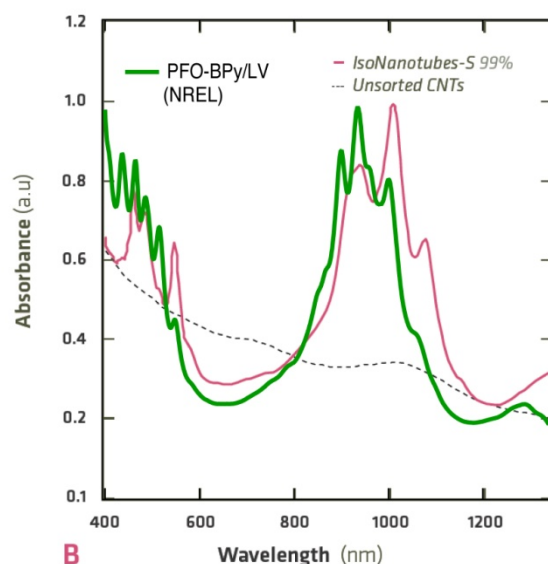
Figure S8. Overlay of PFO-BPy/LV absorbance in toluene with the absorbance of the commercially available IsoNanotubes-S product from Nanointegris. The range for the absorbance axis for the PFO-BPy/LV sample is 0.14 to 1.68.
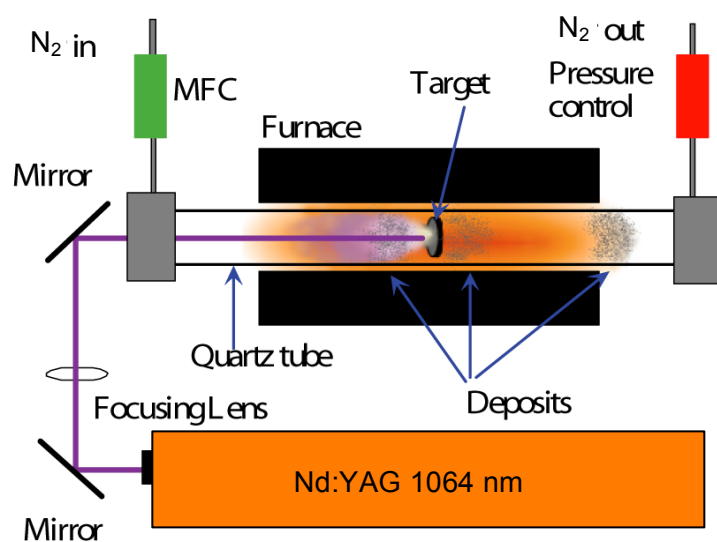

Figure S9. Schematic of the laser vaporization set-up. The temperature of the external furnace controls the synthesis temperature. Our "standard" synthesis is run at a furnace temperature of 1125 °C, whereas syntheses for smaller diameter SWCNTs utilize lower furnace temperatures.
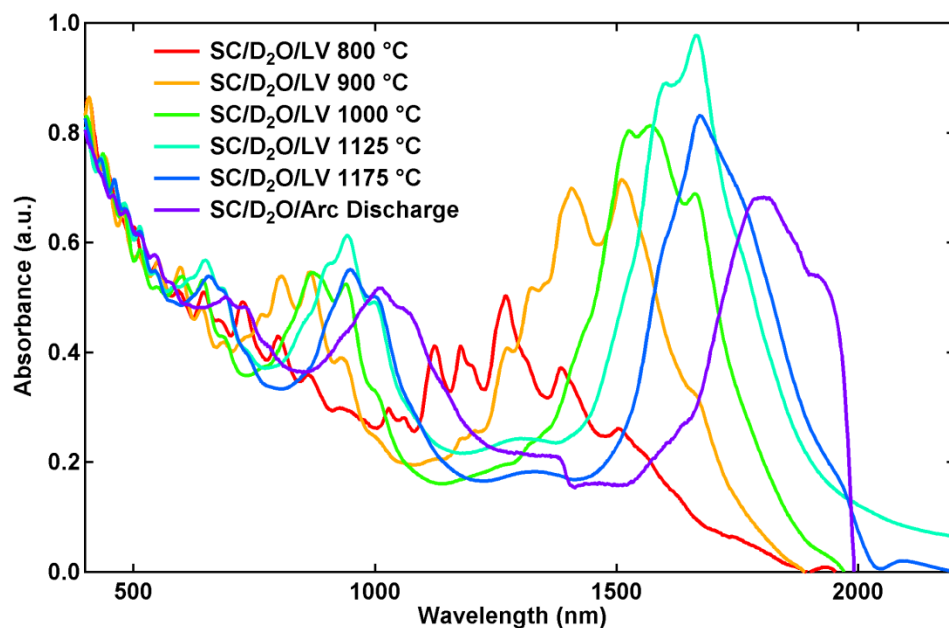
Figure S10. Normalized absorbance spectra of SWCNT starting materials dispersed by SC in D_2O. LV SWCNT diameters increase with higher synthesis temperatures. Commercial arc discharge SWCNTs (NanoLab D1L110-J) provide larger diameter SWCNTs to increase our diameter range.
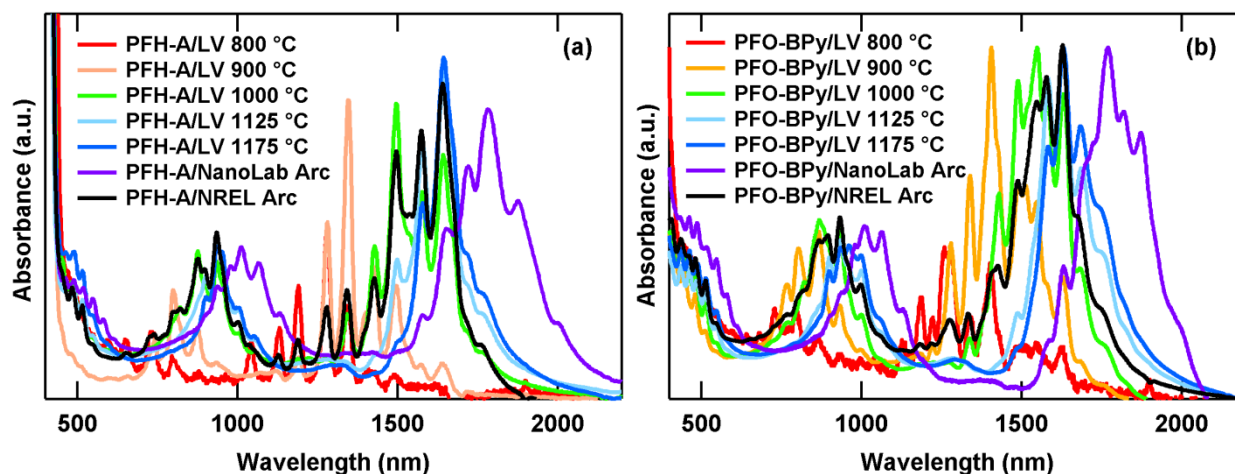

Figure S11. Normalized absorbance spectra for (a) PFH-A dispersions of LV SWCNTs synthesized at different temperatures and two different sources for arc-discharge SWCNTs and (b) the same spectra, but dispersed with PFO-BPy.
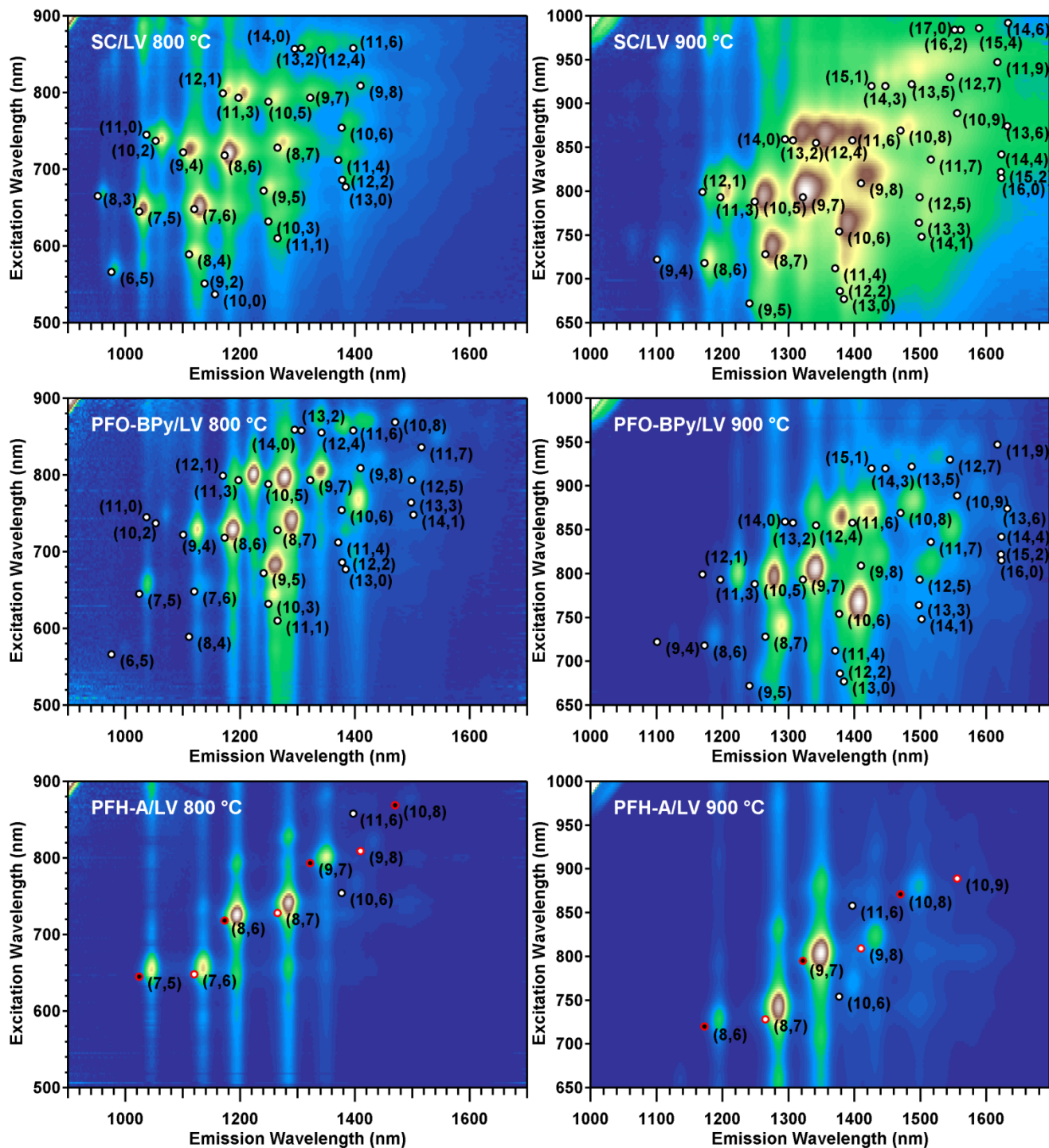
Figure S12. PLE maps for LV SWCNTs synthesized at (left column) 800 °C and (right column) 900 °C. The rows correspond to SWCNTs dispersed in (top row) SC/D$_2$O, (middle row) PFO-BPy/toluene, and (bottom row) PFH-A/toluene. The bottom left distribution, observed for the 800 °C sample, is consistent with that of PFH-A/HiPco.[2] Diagonal features in the upper left corners correspond to excitation light entering the detector.
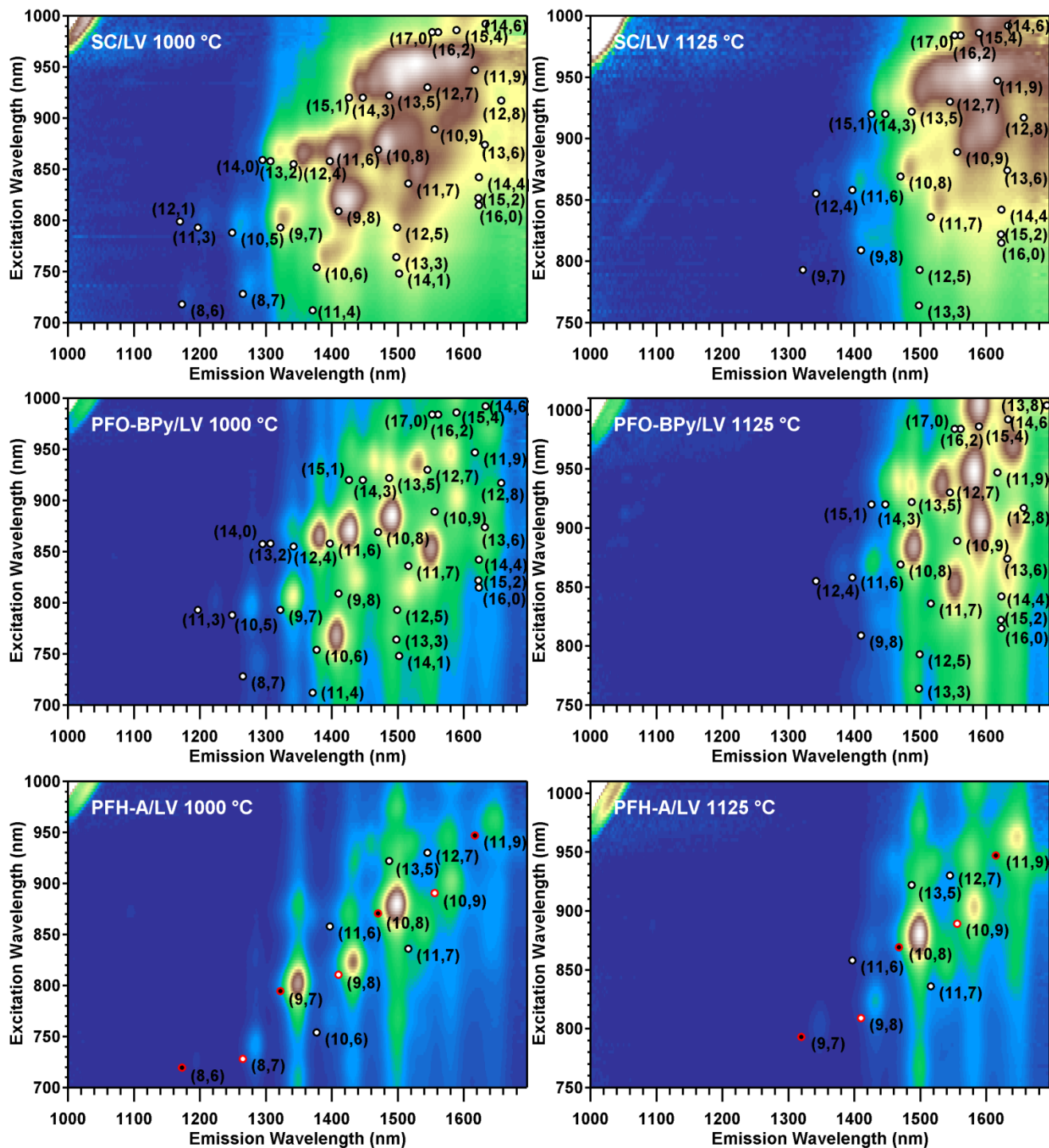
Figure S13. PLE maps for LV SWCNTs synthesized at (left column) 1000 °C and (right column) 1125 °C. The rows correspond to SWCNTs dispersed in (top row) SC/D$_2$O, (middle row) PFO-BPy/toluene, and (bottom row) PFH-A/toluene. Diagonal features in the upper left corners correspond to excitation light entering the detector.

Figure S14. PLE maps for (left column) LV SWCNTs synthesized at 1175 °C and (right column) commercial arc-discharge SWCNTs (NanoLab D1L110-J). The rows correspond to SWCNTs dispersed in (top row) SC/D$_2$O, (middle row) PFO-BPy/toluene, and (bottom row) PFH-A/toluene. Diagonal features in the upper left corners correspond to excitation light entering the detector.
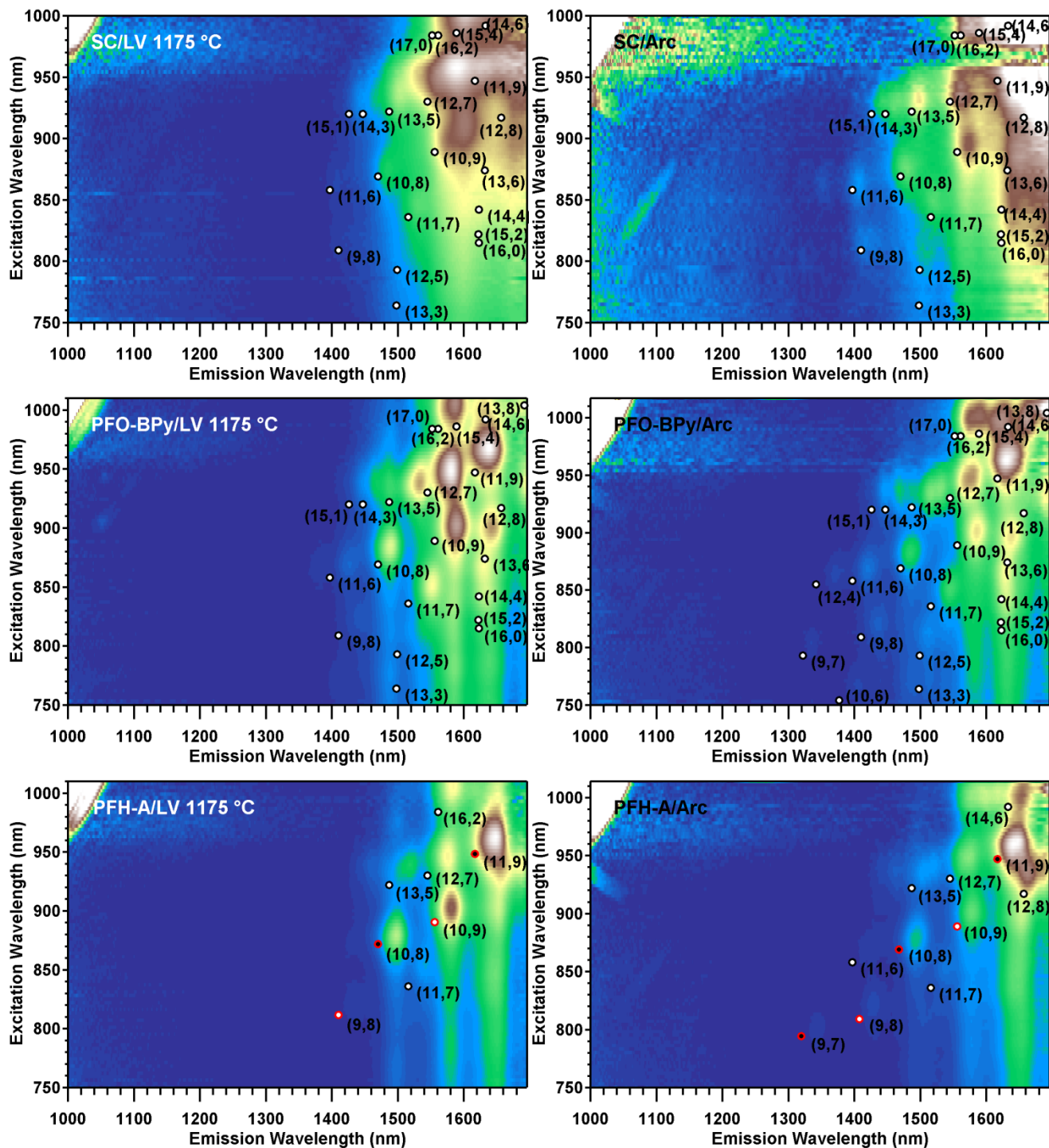
Table of Peak Positions and Shifts for PFH-A and PFO-BPy Dispersions

Chirality	PFO-BPy S11 (nm)	PFH-A S11 (nm)	ΔS11 (nm)	ΔE S_{11} (meV)	PFO-BPy S22 (nm)	PFH-A S22 (nm)	ΔS22 (nm)	ΔE S_{22} (meV)	Diameter (nm)	n-m family
(7,5)	1039	1046	7	-7.99	658	655	-3	8.63	0.829	2
(8,6)	1188	1195	7	-6.11	728	726	-2	4.69	0.966	2
(9,7)	1342	1350	8	-5.47	805	802	-3	5.76	1.103	2
(10,8)	1491	1500	9	-4.99	886	880	-6	9.54	1.24	2
(11,9)	1641	1649	8	-3.67	970	963	-7	9.29	1.377	2
(8,7)	1289	1284	-5	3.75	742	742	0	0.00	1.032	1
(10,6)	1406	1400	-6	3.78	769	770	1	-2.09	1.111	1
(9,8)	1437	1434	-3	1.81	823	824	1	-1.83	1.17	1
(11,6)	1428	1427	-1	0.61	871	871	0	0.00	1.186	2
(11,7)	1551	1540	-11	5.71	853	855	2	-3.40	1.248	1
(13,5)	1532	1518	-14	7.46	937	939	2	-2.82	1.278	2
(10,9)	1589	1581	-8	3.95	904	903	-1	1.52	1.307	1
(12,7)	1581	1577	-4	1.99	946	945	-1	1.39	1.321	2

Table S1. PLE peak positions in PFO-BPy/LV and PFH-A/LV dispersions. The shifts in PFH-A relative to PFO-BPy are also given. The near-armchair SWCNTs are in red. Clear trends are seen in the mod(n − m, 3) = 2 subset of these as explained in the main text. Larger diameter chiralities may be present in some dispersions, but are beyond our current PLE capabilities to quantify.
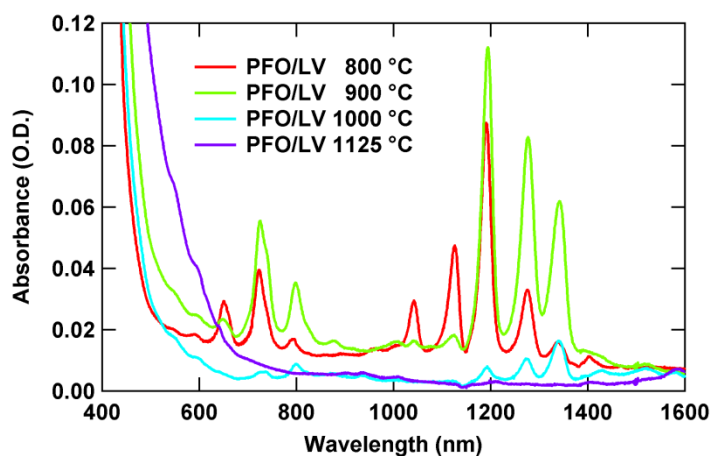

Figure S15. Absorbance spectra for PFO dispersions of LV SWCNTs synthesized at temperatures varying from 800 °C to 1125 °C. At lower synthesis temperatures, the spectra are similar to those from HiPco SWCNTs, but for higher synthesis temperatures, PFO is no longer efficient at selecting near armchair SWCNTs.
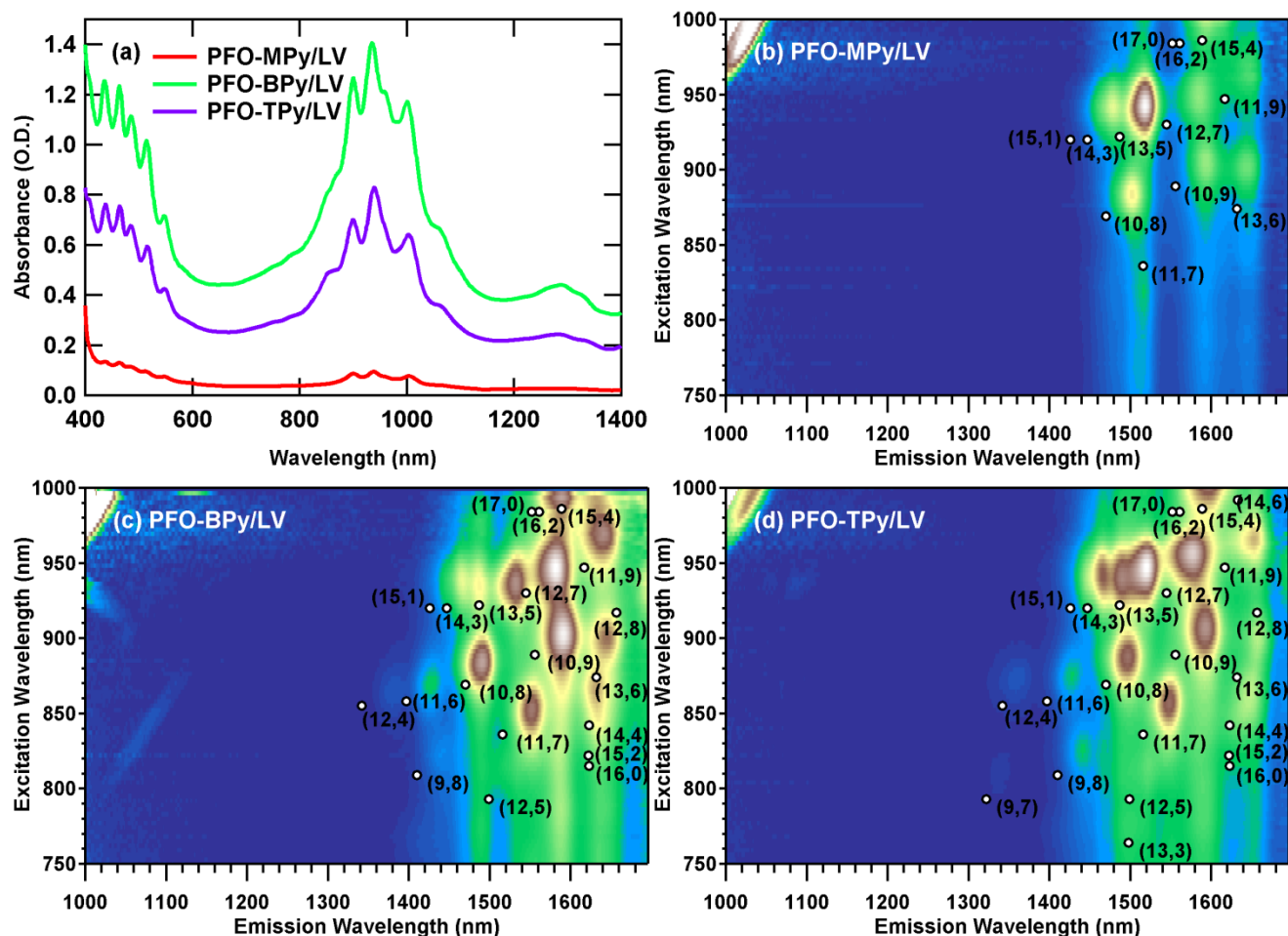
Figure S16. (a) Absorbance spectra of PFO-BPy derivatives with a single pyridine (PFO-MPy, red) and a terpyridine group (PFO-TPy, purple). While not as effective as PFO-BPy, these other two polymers also disperse only s-SWCNTs. (b) PLE map of PFO-MPy/LV. SWCNT dispersions using PFO-MPy are significantly lower yield, but show a preference for (13, 5) nanotubes as recently reported.[3] (c) PLE map of PFO-BPy/LV. (d) PLE map of PFO-TPy. LV synthesis temperature for all three samples was 1125 °C. Polymer and SWCNT loading was the same as in Figures 1 and 5.

Yield and Purity Dependence on Experimental Conditions

Expanding our results to disperse large-diameter s-SWCNTs from any source may play an important role in future applications using these polymers. We explored a number of different experimental factors to determine which ones are important for producing concentrated type-pure semiconducting SWCNTs, namely polymer loading, SWCNT loading, polymer:SWCNT ratio, sonication time, centrifugation time, and SWCNT source.

Higher polymer loading (in our raw LV case, ~2.5 mg/ml) led to more concentrated and higher yield dispersions. If the initial SWCNT loading is too low, having a high polymer loading can lead to m-SWCNTs being dispersed as well. This loading, however, depends on starting SWCNT material (LV vs. arc-discharge, raw vs. purified, and fraction of SWCNTs in material). Thus, it is the polymer:SWCNT ratio that must be tuned based on the starting material. Too high a ratio and metals can begin being dispersed, while too low a ratio leads to lower yields and concentrations. Interestingly, our raw LV SWCNTs could be pushed to a higher polymer loading without acquiring metals than our purified LV (buckypaper) material. The reason for this difference is still unknown, but allows us to skip purification steps that lower yield and are time intensive, while obtaining higher

yield, higher throughput results. As seen in Figure S11, we also dispersed raw commercial arc-discharge SWCNTs (NanoLab D1L110-J) as well as our own raw in-house arc-discharge SWCNTs using loadings of about 1:1 polymer:raw SWCNT material.

Sonication and centrifugation considerations were also made. We found that increasing sonication time from 30 minutes to 1 hour led to higher yields, and behaved similarly to adding extra polymer, *i.e.* it could lead to m-SWCNTs starting to disperse. This allows a tradeoff between throughput (shorter sonication time) and starting material (less polymer). Longer centrifugation did not have a strong effect on our dispersions, but did lead to minor modifications in the chiral distribution. Other minor modifications were observed for lower polymer loadings, but neither of these removed any individual chirality to the point of higher selectivity.

References
(1) Blackburn, J.L.; Holt, J.M.; Irurzun, V.M.; Resasco, D.E.; Rumbles, G. Confirmation of K-Momentum Dark Exciton Vibronic Sidebands Using ^{13}C-labeled, Highly Enriched (6,5) Single-walled Carbon Nanotubes. *Nano Lett.* **2012**, 12, 1398-1403.
(2) Chen, F.; Wang, B.; Chen, Y.; Li, L.-J. Toward the Extraction of Single Species of Single-Walled Carbon Nanotubes Using Fluorene-Based Polymers. *Nano Lett*. **2007**, 7, 3013-3017.
(3) Tange, M.; Okazaki, T.; Iijima, S. Selective Extraction of Semiconducting Single-Wall Carbon Nanotubes by Poly(9,9-dioctylfluorene-alt-pyridine) for 1.5 μm Emission. *ACS Appl. Mat. & Inter*. **2012**, 4, 6458-6462.